Paired Site Characterization in Aluminosilicate Zeolites through Limited Alkylammonium Stability

Ajibola Lawal† and Omar A. Abdelrahman †*

† Department of Chemical Engineering, University of Massachusetts Amherst, 686 N. Pleasant Street, Amherst, MA 01003, USA

*Corresponding Author: abdel@umass.edu

Abstract. The spatial distribution of tetrahedrally coordinated aluminum incorporated into a mordenite framework inverse framework zeolite was investigated through the proton site-selective probe chemistry of alkylamine Hofmann elimination. Protons associated with paired Al sites were exclusively exchanged with divalent cobalt, while isolated protons remained intact and readily quantified through Hofmann elimination of adsorbed alkylammonium species. Through a combination of temperature-programmed methods and spectroscopic characterization, the stability of the adsorbed alkylammonium was found to be crucial to the accurate estimation of isolated protons. Only alkylammonium species undergoing Hofmann elimination through a primary carbocation were found to exclusively probe isolated protons on the surface of cobalt-exchanged ZSM-5. More stable secondary and tertiary carbocations typically used in the characterization of acid sites, resulted in significant overestimates of protonic site densities. The result is contrary to purely protonic zeolites, where alkylammonium stability is inconsequential to the quantification of the acid sites they are coordinated with. Consequently, n-propylamine was found to be a suitable reactive probe molecule for the quantification of isolated protonic sites on divalent metal-cation zeolite surfaces, forming n-propylammonium upon adsorption. Ensuring accurate probing of isolated protons on the surface of metal cation exchanged zeolites was also demonstrated to require control of ion-exchange conditions and sufficient extent of zeolite exposure to the adsorbing n-propylamine. The fraction of paired Al sites in ZSM-5 was measured to systematically increase with Al content, ranging between 6 and 63 % across a Si/Al of 140 and 11.5, respectively. Experimentally measured Al pairing was in excellent quantitative agreement with a binomial distribution, suggesting a random incorporation of Al into the tetrahedral sites of ZSM-5 at next-nearest-neighboring positions.

1. Introduction. The use of heteroatom-substituted zeolites as catalysts,[1-5] adsorbents,[6-10] and membranes[11-15] has provided a valuable platform to impact various parts of the chemical industry. In particular, aluminosilicate zeolites, resulting from the incorporation of an Aluminum atom into a tetrahedrally coordinated position within the otherwise siliceous zeolite framework, have been predominantly used. Incorporation of Aluminum into the framework leads to a charge imbalance, reflected in a negatively charged oxygen bridging the gap between Si and Al, and can be balanced by a large number of cations depending on the desired application. Monovalent metal cations like sodium (Na^+) and lithium (Li^+) afford zeolites are desirable properties for the adsorption-based separation of xylene mixtures [18] and propane/propylene,[19] respectively. A proton can also be leveraged as the balancing cation, creating a Brønsted acidic bridging hydroxyl, that serves as the catalytic backbone for multiple industrial chemistries.[20-24] As a result, a large body of research has been devoted to the study of aluminosilicate zeolites, seeking to understand their catalytic properties through kinetic investigations,[25-29] material characterization,[30-32] and computational calculations.[33-37]

Early research in the field centered on the quantification of the protonic Brønsted acid sites of aluminosilicate zeolites; temperature

programmed,[38-39] spectroscopic,[40-41] and nuclear magnetic resonance[42-44] based methods have all been deployed for acid site quantification. Pioneered by Gorte and co-workers, temperature programmed surface reaction methods, coupled with the Brønsted acid selective Hofmann elimination, lead to accurate and accessible methods for characterizing Brønsted acid site density.[45-48] More recent efforts focused on understanding the consequence of acid site spatial proximity to function; will protonic sites proximal to one another behave differently than those in isolation within the pore of a zeolite? Two framework Al atoms proximal as next-nearest-neighbors are considered to be paired, while a framework Al with no nearest neighbors other than Si is considered to be isolated (**Scheme 1**). The influence of proximate Al pairs has been shown for methanol to aromatics conversion,[49-50] benzene alkylation,[51-52] alkane/alkene cracking,[53-54] olefin aromatization,[55] and alcohol dehydration.[56] For applications involving the inclusion of metal cations at proximate sites, reduced Ga species over Al-pairs have been shown as active centers for alkane dehydrocyclization and dehydrogenation.[57-58] The relevance of Cu balanced by paired sites in zeolites has been investigated for low-temperature ammonia selective catalytic reduction,[59-61] as well as the impact of water vapor for the ion-mediated chemistries over proximate Al-pairs.[62] Al-pairs has also been reported to influence alkane separation,[63] water adsorption,[64] and CO_2 adsorption.[65] As a result, significant effort has been dedicated to understanding the means by which to intentionally synthesize paired Al zeolites. The influence of kinetic factors,[66-67] Si source,[68] Al Source,[68] structure directing agents (SDA)[69-70] have all been investigated. The cations present in the SDAs that balance the charge of the Al^{3+}, plays a role in Al siting within the zeolite.[71] Other work has focused on the nature of the mineralizing agent and synthesis procedure to influence Al distribution in ZSM-5 zeolites.[72] Gounder and co-workers also showed the possibility of using cations like Na^+ as an inorganic SDA, combined with organic SDAs, to synthesize Chabazite with varying fractions of Al pairs.[73]

With the potential for the proximity of Al sites to tune the function of their charge balancing cations, the ability to quantify the fraction of Al sites paired in a zeolite framework was needed. Early efforts by Dědeček,[74-75] built upon by Bell,[76] Gounder,[73, 77-78] and others,[53, 79] relied on divalent metal cations to probe framework incorporated aluminum atoms neighboring each other. Unlike monovalent cations (Na^+, Li^+) that only balance the charge on a single negatively charged framework oxygen, divalent cations (e.g. Cu^{2+}, Co^{2+}) balance the charge of up to

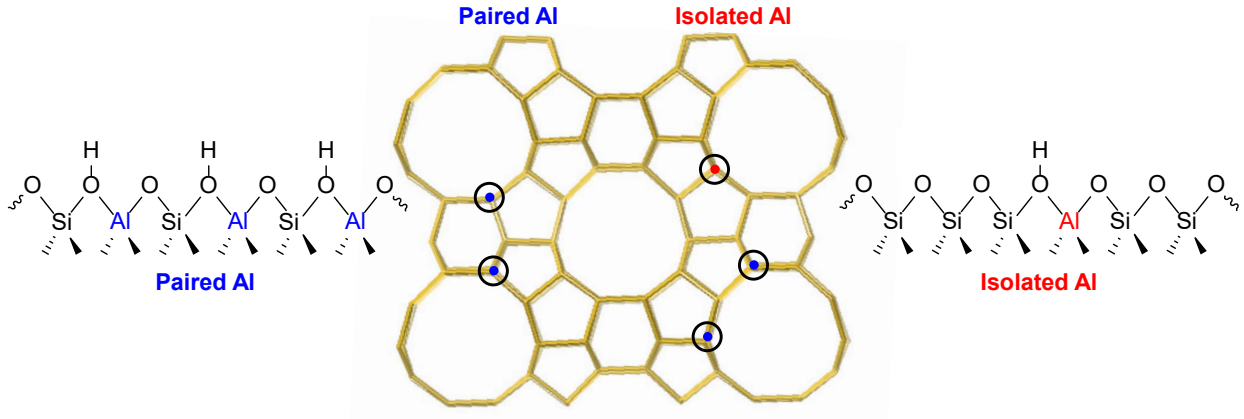

Scheme 1. Spatial identity of Si-Al-OH tetrahedron. Paired and Isolated Aluminum sites, incorporated in a mordenite framework inverted (MFI) structure, determined by the proximity of a framework incorporated Al atom to its next nearest neighbor (NNN).

two negatively charged bridging framework oxygens. If two negatively charged framework oxygens are sufficiently proximal to be accessed by a single unique divalent cation, both negatively charged oxygens can be simultaneously balanced. Quantification of the fraction of framework incorporated Al atoms that can be 'paired' with their next-nearest neighbor (NNN) is reliant on the ability to measure the quantity of divalent cations exchanged. Regardless of whether prior investigations have focused on measuring cation uptake from solution,[80] present on the zeolite surface,[76] or a combination thereof,[78] the use of elemental analysis techniques (emission, atomic absorption, fluorescence etc.) was required. Despite their utility, elemental analysis methods alone do not discriminate between divalent cations interacting with framework species (e.g. anionic oxygen), and those which may be interacting with extra-framework species. A quantitative measure of divalent ions that balance framework oxygens resulting from paired Al sites is needed. Additionally, the cost and level of technical expertise required to perform elemental analysis can be prohibitive, limiting the critical characterization of active site proximity in catalytic studies.

To overcome the challenges associated with existing methods for characterizing active site proximity in heteroatom substituted zeolites, we developed a readily applicable, reactive probe chemistry method that provides chemical specificity (**Scheme 2**). Merging the use of Co^{2+} as a divalent cation to occupy paired sites, and Hofmann elimination-based temperature programmed methods we have previously demonstrated,[81] the fraction of Al pairs present in aluminosilicate zeolites was accurately and reproducibly quantified. Under appropriate solution phase ion-exchange conditions with H-ZSM-5, Co^{2+} exchanges the protons of two neighboring bridging hydroxyls, while isolated bridging hydroxyls remain in their protonic form. The remaining isolated bridging hydroxyls were probed with chemical specificity by adsorbed primary alkylamines, quantified via Hofmann elimination-temperature programmed surface reaction (HE-TPSR). While all primary alkylamines form alkylammonium species once adsorbed on protonic sites, only those forming a primary carbocation (e.g., n-propylamine) were found to be appropriate for chemically probing isolated sites. The measured fraction of Al pairs in H-ZSM-5 was found to be in excellent agreement with predictions based on a statistical Poisson distribution of paired Al sites in a MFI aluminosilicate zeolite, over a large range of Al content (Si/Al = 11.5-240).

2. Experimental methods

2.1. Materials. n-propylamine (99+%, ThermoFisher Scientific), Isopropylamine

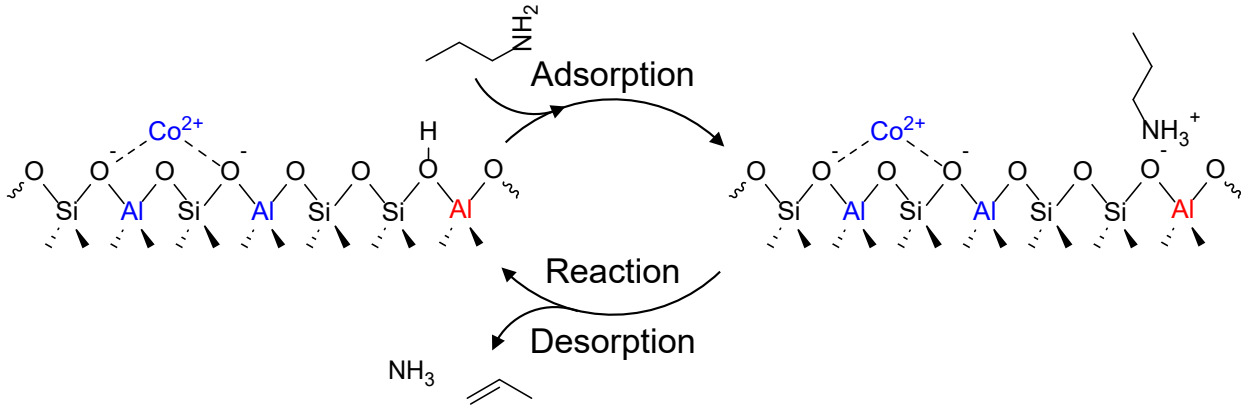

Scheme 2. Chemical Probing of Isolated Protons on Co-ZSM-5. Adsorption and subsequent reaction/desorption of n-propylamine through Hofmann elimination to propene and ammonia over un-exchanged H^+ sites from isolated Al in Co-exchanged zeolites that exchanges divalent Co^{2+} on Al-pairs.

(99%, Acros Organics), tert-butylamine (99.5%, Sigma Aldrich), pyridine (≥99.9%, Sigma Aldrich) and propene (0.86 mol% in nitrogen, Gasco) were used as probe molecules and/or for instrument calibration. He (99.999%, Airgas), Ar (99.999%, Airgas), N_2 (99.999%, Airgas), and Air (Ultra-zero, Airgas) were used as carrier gas and for zeolite pretreatment. Ammonium form ZSM-5 (CBV2314, Si/Al = 11.5; CBV3024E, Si/Al =15; CBV5524G, Si/Al = 25; CBV8014, Si/Al = 40; CBV28014, Si/Al = 140) was obtained from Zeolyst, Si/Al = 240 was obtained from Acros Organics (ZSM-5, 279575000). Sodium chloride (99 %, Sigma Aldrich) and Cobalt (ii) nitrate hexahydrate (99 %, Acros Organics) were used to prepare aqueous ion-exchange solutions. Type 1 water (> 18.2 MΩ-cm) used in the preparation of metal-cation zeolites was generated using an in-house purifier, equipped with particulate filtration, reverse osmosis, and ion-exchange filters (Spectrapure).

2.2. Zeolite pretreatment. Ammonium-form (NH_4^+) ZSM-5 was converted to its hydrogen form (H^+) by ex-situ calcination in a custom tubular setup. Typically, 0.5 g of zeolite was loaded into a downflow U-shape quartz tube, heated in a tube furnace (GSL-1100X, MTI Corporation) under a 100 sccm flow of air (Ultra-zero, Airgas) regulated using a mass flow controller (5850S, Brooks Instrument). A plug of deactivated glass wool (24324, Restek) was placed at the bottom of the quartz U-tube as a physical support for the zeolite bed. All zeolite powders were calcined at 823 K for 10 h with a ramp rate of 2 K min^{-1}; to ensure accurate calcination temperatures, a 1/16″ type-K thermocouple (KQXL-116G-12, Omega) encased within a quartz sheath was placed in direct contact with the zeolite. Details of the ex-situ calcination system are provided in the Supporting Information (**Sec. S1**). Calcined zeolites were stored in a desiccator to limit exposure to atmospheric moisture.

2.3. Ion Exchange. Zeolites were converted to their sodium and cobalt forms using established ion-exchange procedures to replace protons on isolated and/or paired Al sites. [73, 76, 78] 0.1 g of H-ZSM-5 was added to a 0.5 M metal-cation aqueous solution (150 cm^3 solution g.zeolite $^{-1}$) in a 100 ml round bottom flask, equipped with an overhead condenser with an internal flow of ambient water to limit concentration changes through evaporation. The solution was held constant at a desired temperature for 24 hours, measured with a quartz sheath encased thermocouple (KQXL-116G-18, Omega) in solution, under continuous stirring (14-513-98, Fisher Scientific) with a heated stir plate (6795-220, Corning). Ion-exchanged samples were then washed four times in Type 1 water and dried in a natural convection oven (13-247-650G, Fisher Scientific) at 373 K for 24 hours, before calcination in a quartz U-tube setup (**Sec. 2.2**) at 773 K for 6 hours with a ramp rate of 1 K min^{-1} under a 100 sccm flow of air.

2.4. Spectroscopic Characterization. In-situ Fourier transform infrared (FT-IR) spectroscopy was performed using a Bruker Tensor II spectrometer equipped with a DLaTGS detector and mid-IR source. Spectra were recorded between 1000 and 6000 cm^{-1} with a 4 cm^{-1} resolution, averaged over 64 scans and subtracted from a background spectrum. Thin self-supporting zeolite wafers were prepared by pressing 10−15 mg cm^{-2} of finely ground zeolite powder in a pellet press at 20 MPa of pressure for 15 minutes. The wafer was then transferred to a custom-built heated transmission cell, equipped with water-cooled CaF_2 windows. The temperature of the cell was controlled using a PID temperature controller (CN 7823, Omega) and a 1/16″ type-K thermocouple, while a secondary thermocouple in a thermowell near the self-supporting wafer was used to measure its temperature. The wafer was first calcined in-situ in 60 sccm of air at 673 K for 1 hour using a ramp rate of 3 K min^{-1},

after which it was cooled down to the desired temperature. Liquid-phase probe molecules were fed to a vaporization section through a 1/16″ PEEK capillary line (0.01″ I.D., TPK110, Vici Valco) using a syringe pump (Masterflex EW-74905-04, Cole-Parmer) and air-tight glass syringe (Hamilton Company). The vaporized liquid was constantly swept by a stream of He passed through a moisture trap (22014, Restek), the flow of which was adjusted using mass flow controllers (Type 201, Porter). The vapor mixture was directed to either the heated transmission cell or a bypass line using a six-port switching valve (A26UWE, Vici Valco) placed within a heated valve enclosure (HVEB, Vici Valco). Any tubing downstream of the vaporization section was heat-traced using resistively heated Nickel Chromium wire (8880K77, McMaster) to avoid condensation, insulated with high-temperature wrap sleeving (6811A11, McMaster).[47, 82]

2.5. Reactive Gas Chromatography. A commercially available quartz GC inlet liner (Agilent 5188-5365) was used as an alkylamine Hofmann elimination microreactor. The liner was packed with a zeolite (supporting information, **Figure S2**), held between two plugs of quartz wool. The quartz wool served as an inert physical support and dispersant to efficiently vaporize injected liquid titrants prior to contacting the zeolite bed. Briefly, the zeolite-containing quartz liner is placed in the inlet of a gas chromatograph (7890B Agilent) equipped with a flame ionization detector (FID). Calcined zeolite powders were pressed, crushed, and sieved to obtain a particle diameter >500 μm; smaller particle diameters were avoided to minimize the pressure drop across the bed. Briefly, 100 mg of the calcined zeolite was loaded into a pellet press (13 mm diameter, Pike Technologies) and pressed at 20 MPa of pressure using a hydraulic press (YLJ-5-H, MTI Corporation). The zeolite pellet was then broken into smaller particles using a mortar and pestle (89037-488, VWR) and sieved (EW-59985-13 and EW-59985-18, Cole Parmer) to obtain the desired sieve fraction. A range of 5 – 30 mg of pelletized zeolite was loaded into the inlet liner microcatalytic reactor; however, 20 mg was typically used. To ensure accurate mass loadings, the mass of the entire microreactor packed with deactivated quartz wool was measured before and after adding the zeolite.

Once placed in the inlet, the microcatalytic reactor was calcined in air at 673 K for one hour with a ramp rate of 10 K min^{-1} to remove any carbonaceous deposits or moisture. Effluent air from the liner was routed through a heated six-port valve, which bypassed the GC column and sent flow from the inlet directly to the detector. A purge stream of N_2 was directed to the GC column (PLOTQ, 19091-Q04) through the same six-port valve, ultimately sent to an atmospheric vent line. Once calcined, the liner was purged with N_2 and cooled down to 423 K and held for thirty minutes to ensure an equilibrated bed temperature. The zeolite was then exposed to the probe molecule using an automated liquid sampler (ALS); a continuous stream of probe molecule was introduced using the ALS to dispense at a fixed volumetric flowrate. Argon then swept the vaporized probe molecule, bringing it into contact with the zeolite bed. The bed was purged under a flowing stream of Ar at 423 K for two hours to remove any excess and/or weakly adsorbed probe molecules. Zeolites were exposed to an excess of probe molecule (~150 mol of probe molecule per mol of bulk Al) to saturate all available sites. Ensuring that all protonic sites were saturated with a probe molecule is further discussed in **Section 3.6**.

Prior to raising the temperature of the zeolite in the inlet liner, the temperature of the GC oven containing the chromatographic column was lowered to 303 K. The position of the six-port valve (6-PV) was also switched such that the N_2 carrier gas passing through the liner, was routed through the GC column first

before reaching the GC-FID detector. Directing the microcatalytic reactor effluent through the GC column at a low temperature, along with a suitable choice of column stationary phase, trapped desorbing molecules from the zeolite surface. The temperature of the microcatalytic reactor was then ramped at a rate of 10 K min^{-1} to 673 K and held for 30 minutes, allowing for the adsorbed alkylamines to either desorb intact or undergo a Hofmann elimination to their respective alkene and ammonia. The temperature of the GC column, containing the trapped molecules, was raised from 303 to 543 K at a ramp rate of 10 K min^{-1} and held there for 10 minutes. An alkene peak corresponding to the alkylamine titrant used was detected and quantified to give a direct measure of the moles formed, which was normalized by the mass of zeolite loaded in the inlet liner microcatalytic reactor to yield a Brønsted acid site density (S_{H+}),

$$S_{H^+}\ (\text{mol g}^{-1}) = \frac{\text{mol Alkene formed (mol)}}{\text{mass of zeolite (g)}} \quad (1)$$

2.6. Temperature-Programmed Surface Reaction. Temperature-programmed surface reaction (TPSR) was performed in a 1/2″ quartz downflow packed bed reactor, with the zeolite bed resting on a plug of deactivated quartz wool. The reactor was placed within a ceramic furnace (VF-360-1.5-6-S, Thermcraft) which was controlled using a PID temperature controller (CN 7823, Omega) and a 1/ 16″ thermocouple encased in a quartz sheath, placed on top of the bed. The entire heated reactor assembly was housed within a larger forced convection oven (5890 Series II, Hewlett Packard) held at 373 K. Liquid-phase probe molecules were fed to a vaporization section through a 1/16″ PEEK capillary line (0.01″ I.D., TPK110, Vici Valco) using a syringe pump (Masterflex EW-74905-04, ColeParmer) and air-tight glass syringe (Hamilton Company). The PEEK line was then connected to a 1/16″ stainless-steel capillary line (0.01″ I.D., T50C10D, Vici Valco) through a PEEK union (ZU1FPK, Vici Valco), and the other end of the stainless-steel capillary line was placed inside the oven. The vaporized liquid was constantly swept by a stream of He, the flow of which was adjusted using a mass flow controller (5850S, Brooks Instrument).

Zeolites were calcined in-situ under 60 sccm of air at 823 K for 4 hours with a ramp rate of 5 K min^{-1} and then cooled to 373 K under the same flow rate of air, before purging in 100 sccm of He for 15 minutes. Zeolites were first saturated with a 1.3 kPa probe molecule-containing stream of He (100 sccm) at 373 K for 10 minutes, then purged in He for 4 hours to remove any weakly adsorbed molecules. Once purged, the bed was ramped to 873 K at 10 K min^{-1} under a 200 sccm stream of He. The effluent concentration of unreacted alkylamine and Hofmann elimination desorbing from the surface were tracked with an online residual gas analyzer (XT200M, ExTorr), while the in-situ bed temperature was recorded with a computer logging temperature controller (CN 7823, Omega).

2.7. Distribution of Paired Sites. The estimation of Al framework distribution, resulting in isolated and paired Al, stems from understanding tetrahedrally coordinated locations (T-sites) within an aluminosilicate unit cell. Starting with a central Al atom, the avoidance of Al-O-Al linkages per Löwenstein's rule dictates that all next-neighboring (NN) framework positions be occupied by Si,[16-17] beyond which twelve unique T-sites are occupied by aluminum or silicon as the next-nearest-neighbor (NNN, **Scheme 3**). The probability of siting Al at a (NNN) T-site and forming an Al-pair is directly correlated with the relative molar content of framework incorporated silicon and aluminum (Si/Al), which is quantitatively described by the binomial distribution (P_n) of NNN T-sites occupied by Al,

$$P_n = \binom{N_T}{n} \left(\frac{1}{Si/Al}\right)^n \left(\frac{Si/Al-1}{Si/Al}\right)^{N_T-n} \quad (2)$$

where N_T is the average number of T-sites available within each unit cell, reported to be a value of 11.8 for MFI,[83] slightly lower than the twelve theoretically available T-sites due to adjacent Si atoms sharing one next-nearest-neighboring site. 'n' is the number of NNN T-sites occupied by aluminum.[83]

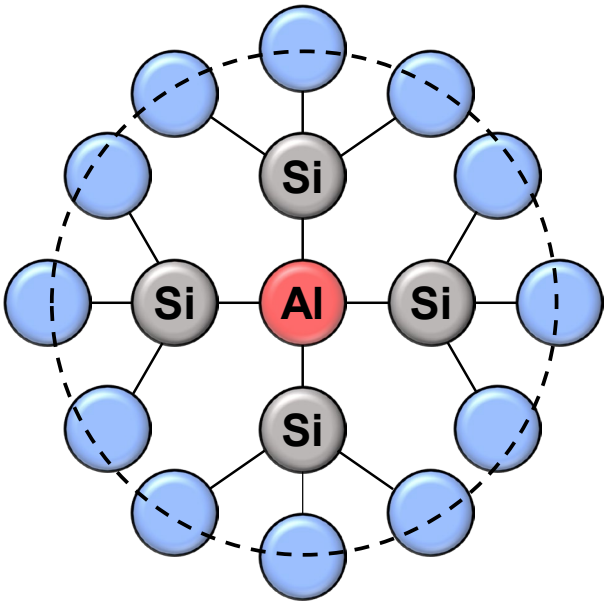

Scheme 3. Relative Distribution of Tetrahedrally Coordinated Aluminum and Next Nearest Neighbors. Relative to the position of a **central Al atom**, surrounded by four silicon atoms as the nearest neighbor, with **twelve unique T-sites** that can be occupied by another Al or Si atom as the next-nearest-neighbor (NNN). Oxygen linkages between neighbors is implicitly assumed.

At a given Si/Al molar ratio, when no Al is sited at any available NNN T-sites (n = 0), the probability of forming an aluminosilicate with only isolated Al sites can be calculated (P_0). The fraction of framework Al paired with its next-nearest neighbor ($f_{Al,Pairs}$) can therefore be calculated,[84]

$$f_{Al,Pairs} = 1 - P_0 = 1 - \binom{N_T}{0}\left(\frac{Si/Al-1}{Si/Al}\right)^{N_T} \quad (3)$$

Experimentally, the fraction of Al pairs ($f_{Al,Pairs}$) was estimated by measuring the Brønsted site density (S_{H+}) of Co-exchanged zeolites, representing the fraction of protons on isolated framework incorporated Al, normalized by the Brønsted site density (S_{H+}) of the parent protonic form zeolite,

$$f_{Al,Pairs} = \frac{S_{H^+,H\text{-}Zeolite} - S_{H^+,Co\text{-}Zeolite}}{S_{H^+,H\text{-}Zeolite}} \; [=] \; \frac{\text{mol } H^+ \text{on paired Framework Al}}{\text{mol } H^+ \text{on Framework Al}} \quad (4)$$

where $S_{H+,H\text{-}Zeolite}$ and $S_{H+,Co\text{-}Zeolite}$ are the measured Brønsted site densities (mol H^+ g zeolite^{-1}) on the H-form and Co-form zeolite, respectively, where their difference is equal to the density of protons associated with pairs of framework incorporated Al. The density on the parent zeolite represents protons stemming from both isolated and paired framework incorporated Al sites.

3. Results & Discussion. The siting of Al within an aluminosilicate zeolite was assessed for an MFI framework, a range of Si/Al ratios were considered to probe the effect of Al content (Si/Al = 11.5 – 240, **Table 1**). The MFI framework offered the advantage of mitigating the influence of extra-framework Al, where prior work has established the near-complete framework incorporation of Al. [85-88] The average MFI pore diameter (~ 5.5 Å) [89-90] also afforded the ability to consider a range of solid acid probe molecules, without steric constraints or the inability of a probe molecule to physically access a Brønsted acid site. Over Al content range considered (Si/Al), the expected Al content per unit cell of the zeolite (Al/UC), fraction of Al pairs expected based on a statistical distribution ($f_{Al,pairs}$, calculated) and measured ($f_{Al,pairs}$, Measured), and resulting extent of Cobalt exchange (Co^{2+}/Al_{tot}) are reported in **Table 1**. Comparing the density of protonic sites available on the parent H-ZSM-5 zeolite relative to the bulk Al content (H^+/Al_T), suggests near-complete framework incorporation of Al across the various zeolites.

Table 1. Physical and Chemical Properties of Commercially Sourced ZSM-5

Framework	Si/Al[a]	Al/UC[b]	H^+/Al_T [%][c]	Co^{2+}/Al_T [%][d]	$f_{Al,pairs}$ [%]	
					Measured[e]	Calculated[f]
MFI	11.5	7.7	100	31.5	63	66
MFI	15	6.0	80	26.0	52	56
MFI	25	3.7	93	16.0	32	38
MFI	40	2.3	130	17.5	35	26
MFI	140	0.7	99	3.0	6	8
MFI	240	0.4	106	6.0	12	5

a- Bulk Si/Al ratio reported by vendor (Zeolyst, Acros Organics)
b- Calculated using MFI unit cell formula; Al/UC = 96/(1+Si/Al)
c- Estimated from measured Brønsted acid site density (Eq. 1) relative to bulk Al content ($Al_T = (Al/Si)/MW_{SiO2}$)
d- Measured fraction of protonic sites exchanged with Co^{2+} at 353 K
e- Measured fraction of Al-pairs based on residual S_{H^+} density of Co^{2+} exchanged zeolite (Eq. 4)
f- Calculated fraction of Al-pairs assuming a random binomial distribution of framework aluminum (Eq. 3)

3.1. Alkylamine Identity. Alkylamines have been established as appropriate probe molecules for estimating the Brønsted acid site density of aluminosilicate zeolites. [48, 81, 91-92] Alkylamines stoichiometrically adsorbed on H^+ sites (ZOH) as alkylammonium ion complexes (1 mol RNH_2 per mol H^+), that undergo Hofmann Elimination at elevated temperatures to form their corresponding alkene(s) (R') and ammonia (1 mol alkene + NH_3 per mol RNH_3^+), [47-48, 91] providing a direct measure of the moles of H^+ sites accessible to the alkylamine,

$$RNH_2 + ZOH \rightharpoonup RNH_3^+ \cdots {}^-OZ \quad (5)$$

$$RNH_3^+ \cdots {}^-OZ \rightleftharpoons R' + NH_3 + ZOH \quad (6)$$

It is worth noting that alkylamine adsorption on a protonic site can be treated as irreversible (Eq. 5), where the alkylamine only desorbs reactively through Hofmann elimination (Eq. 6). Conversely, when a monovalent cation like sodium (Na^+) is introduced to a proton form zeolite, exchanging all available H^+ sites (paired and isolated), all Brønsted acid catalyzed chemistry is expected not to proceed. [93-97] In the absence of a sufficiently acidic proton on the surface, an alkylamine will molecularly desorb intact, as opposed to reactively desorbing through Hofmann elimination. Therefore, the extent of ion exchange was investigated by measuring residual H^+ sites using alkylamine Hofmann elimination (reactive gas chromatography, **Sec. 2.5**).

For the parent H-ZSM-5, we have previously reported no difference in the measured Brønsted acid site density based on n-propylamine (NPA), isopropylamine (IPA), and tert-butylamine (TBA), regardless of Al content. [81] Conversely, over Na-ZSM-5, a trend is observed with respect to the fraction of Brønsted acid sites measured relative to the parent H-ZSM-5 (**Fig. 1)**. Based on n-propylamine as a probe molecule, the majority of protons appear to have been exchanged with

Na (> 96%). With isopropylamine and tert-butylamine, the apparent fraction of residual H^+ measured increased to 14 and 61%, respectively. Regardless of Al content (Si/Al = 11.5 and 140), similar trends were observed across the three alkylamine probe molecules.

Despite the varying observations based on three distinct alkylamines (NPA, IPA, and TBA), the true extent of Na^+ exchange on the zeolite surface cannot be different. While sterics can explain differences in reactivity amongst distinct probe molecules, [98-101] n-propylamine is the least sterically hindered, yet experienced the smallest extent of Hofmann elimination over Na-ZSM-5. Another distinction between the alkylamine probe molecules is the stability of the carbocation formed in the course of Hofmann elimination, [47, 102] dictated by the degree of substitution of the alpha carbon (C_α). We have previously demonstrated that a more substituted alpha carbon facilitates the ease with which alkylamine Hofmann elimination proceeds, as a result of a more stable carbocation. [103] The stability of the carbocation formed by the three alkylamines increased in the order of NPA < IPA < TBA, with alpha carbon of TBA forming the most stable carbocation. Highly substituted alkylamines like tert-butylamine may therefore undergo Hofmann elimination over an aluminosilicate as a result of a more stabilized alpha carbocation, even in the absence of a protonic bridging hydroxyl, underestimating the extent of ion exchange. Given the desire to probe only residual H^+ not exchanged by a metal cation through Hofmann elimination, n-propylamine is a more suitable reactive probe molecule, revealing complete H^+ site exchange with Na^+. The observation based on NPA of near-complete Na exchange also holds for other 1º alpha-carbon (C_α) substituted alkylamines; the measured fraction of H^+ exchanged measured after Na-ion exchange is comparable with n-butylamine and n-amylamine (≥ 92 %, Supporting information, **Figure S3**). While IPA and TBA are suitable probes for H-form zeolites, differences observed for Na-ZSM-5 highlights the importance of an appropriate probe for the characterization of ion-exchanged aluminosilicates.

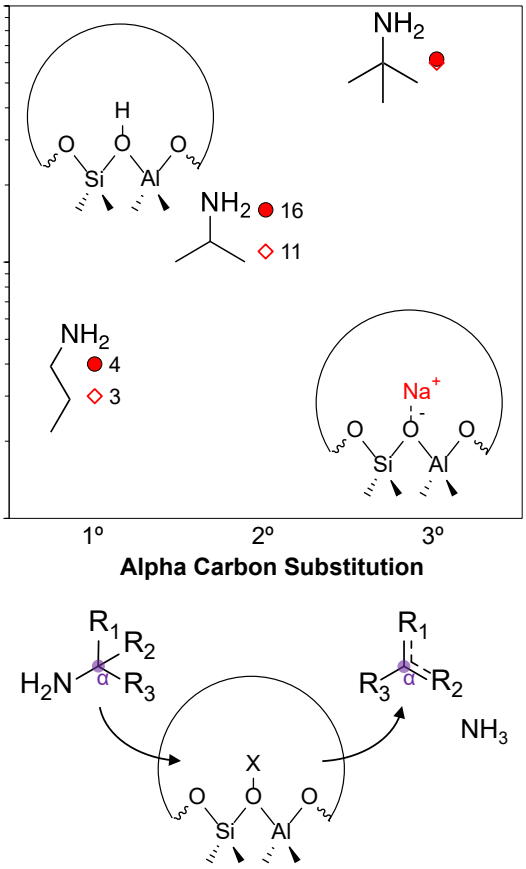

Figure 1. Degree of Na Exchange. Relative Brønsted acid site (BAS) density of Na-exchanged and **protonic form** ZSM-5 (Si/Al = 11.5 ●, 140 ◊), measured by Hofmann elimination TPSR of alkylamines with varying alpha carbon (α) substitution.

3.2. Temperature Programmed Surface Reaction. Having identified n-propylamine as a more selective molecular probe for H^+ sites in Na-exchanged zeolites, we sought to understand the nature of the adsorbate-adsorbent interaction, and the ultimate decomposition of the molecular probe through

Hofmann elimination over Co exchanged zeolites. If Co was only to exchange H^+ sites resulting from paired Al sites, n-propylamine should only probe residual isolated H^+ sites over Co-ZSM-5. In **Figure 2A,** the TPSR of n-propylammonium on MFI zeolites in their H, Co, and Na forms is shown, where the desorption of propene from the various zeolites was tracked. No significant NPA Hofmann elimination products were desorbed from the surface of Na-ZSM-5, further confirming the exchange of H^+ sited on paired and isolated Al sites with monovalent Na^+ (**Figure 1**). A similar range of peak temperatures for propene desorption from H-ZSM-5 (670 K, Si/Al = 11.5) and Co-ZSM-5 (699 K, Si/Al = 11.5) was observed, consistent with peak desorption temperatures previously reported for the TPSR of NPA adsorbed on H-ZSM-5 (675 K). [47] The similar Hofmann elimination TPSR profiles for Co and H-ZSM-5 suggested that n-propylamine only probed protonic sites on both zeolite surfaces. We have previously demonstrated that the kinetics of alkylamine Hofmann elimination is insensitive to Al content for a given zeolite framework, [103] consistent with the similar propene peak desorption temperatures observed here. The moles of propene evolved from the surface of Co-ZSM-5 through Hofmann elimination, however, was 63 % lower relative to the parent H-ZSM-5. The partial decrease in the extent of Hofmann elimination over Co-ZSM-5, as opposed to almost complete absence over Na-ZSM-5, is attributed to Co as a divalent cation only exchanging protons from paired Al sites. The observed propene evolution over Co-ZSM-5 is attributed to the Hofmann elimination of NPA adsorbed on isolated protonic sites, not exchanged by Co^{2+}.

3.3. Fourier Transform Infrared Spectroscopy of Pyridine (Py-IR). While consistent with the exchange of H^+ located at paired and/or isolated Al sites with Na^+ and Co^{2+}, it is unclear whether the reduced fraction of available H^+ over metal cation exchanged ZSM-5 is a result of hindered Hofmann elimination, or that H^+ sites are no longer available to protonate a basic probe molecule. To help distinguish between the two possibilities, the spectroscopic signature of pyridinium ions formed when pyridine adsorbs on a sufficiently acidic protonic site was leveraged. [104-106] Specifically, the N-H bending vibrational frequency of surface pyridinium (1545 cm^{-1}) and the Lewis acidic type interaction at ~1450 cm^{-1} were investigated on H-ZSM-5, Co-ZSM-5, and Na-ZSM-5 (**Figure 2B**). Pyridine IR of zeolites is routinely employed to investigate the presence or absence of H^+ sites; [41, 104, 107-108] the specific N-H bending vibration that observed from the formation of surface pyridinium ions (Py^+) details the exclusive interaction of H^+ sites with basic pyridine. [109-110] The intensity of the pyridinium peak at 1545 cm^{-1} was highest with the H-form zeolite where all available H^+ sites protonated the adsorbing pyridine, followed by the Co-form, where only a fraction of protons had been exchanged, and lastly the Na-form. No significant Lewis interactions were observed over the H-form, likely due to the minimal extra framework Al present in the MFI framework. [76] Conversely, significant Lewis acid-base interactions were observed on both Co (1451 cm^{-1}) and Na (1443 cm^{-1}) form zeolites.

The absence of any significant pyridinium formation on Na-ZSM-5, combined with the appearance of distinct Lewis-type interaction at 1443 cm^{-1}, further confirmed the near-quantitative exchange of H^+ sites with monovalent Na^+. Similarly, for Co-ZSM-5, the reduced formation of pyridinium is consistent with a divalent cation preferentially exchanging protons located on paired Al sites. The metal cation exchange was further evidenced by the bridging hydroxyl peaks at 3605 cm^{-1}, representative of protonic sites resulting from framework incorporated Al, which were partially and fully absent on Co and

Na-ZSM-5, respectively (**Figure S5**). Interestingly, the silanol peak at 3740 cm^{-1} appeared relatively unchanged for all zeolite forms (H, Na, and Co), suggesting that cations preferentially exchanged protons originating from the aluminosilicate framework's bridging hydroxyl (**Figure S5)**.

3.4. Fraction of Protons Exchanged. Similar fractions of exchanged protons were quantified through NPA Hofmann elimination, and the N-H bending peak associated with adsorbed pyridinium at 1545 cm^{-1} (**Figure 2C**). For monovalent Na^+, near quantitative exchange of all available H^+ sites was observed based on NPA Hofmann elimination (96%) and Py-IR (94%). For divalent Co^{2+}, 63 and 50% of all available H^+ sites were found to be exchanged based on NPA-RGC, and Py-IR, respectively. The fraction of protons exchanged for Co^{2+}, equivalent to the fraction of paired Al sites, suggests that ~2/3 of Al sites in the MFI framework (Si/Al = 11.5) are paired. We note that the measured fraction of Al pairs (63%) is consistent with the predictions based on a random statistical distribution of framework Al (Eq. 3, 66%), and similar to what has been measured by Bell and co-workers (56 %, Si/Al = 11.5) through elemental analysis of the exchanged zeolite.[76]

3.5. Ion-Exchange Conditions. Having established NPA as a suitable molecule to quantitatively probe the fraction of protons not exchanged in Co-ZSM-5, we investigated the influence of ion-exchange conditions. Given that ion-exchange is a reversible reaction, chemical equilibrium can be shifted through temperature, [111-113] to ensure complete cation exchange of all available H^+ sites on the zeolite surface. Considering monovalent Na^+, where complete proton exchange is expected, only ~75% of available protons were exchanged at ambient temperature (**Figure 3A**). Increasing the temperature at which ion-exchange was performed resulted in almost complete proton exchange; 96 % of all available protons in H-ZSM-5 (Si/Al = 11.5) were exchanged with Na^+ at 353 K. The effect of temperature on ion exchange has been evaluated by Gounder and co-workers, where they showed an increased exchange of Co^{2+} at 353 K relative to 298 K, and determined the higher temperature to be sufficient to exchange Co^{2+} into all available paired sites. [114] Dědeček and co-workers also found the necessity for above ambient

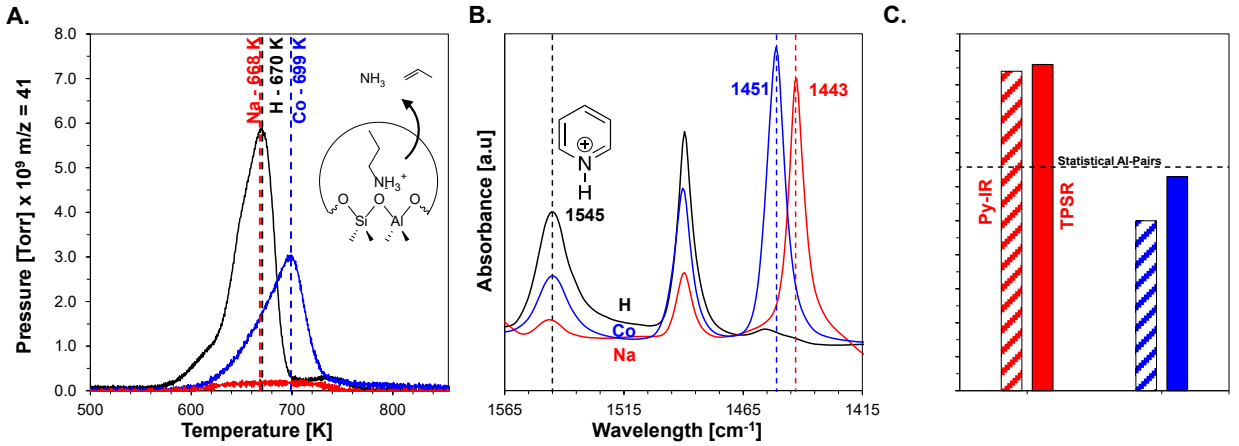

Figure 2. **Na and Co ion exchange with H-ZSM-5 A.** Temperature programmed surface reaction of n-propylamine to propene (m/z = 41, Si/Al = 11.5) and **B.** FT-IR spectra of pyridine adsorbed on **protonic (H)**, **sodium (Na)**, and **cobalt (Co)** exchanged ZSM-5 (Si/Al = 11.5) **C.** Fractions of protons exchanged measured by the moles of propene evolved during n-propylamine TPSR from H-ZSM-5 relative to metal cation-exchanged, and the relative area of the pyridinium ion (1545 cm^{-1}) interaction over the same materials (Py-IR). The dashed line represented the calculated fraction of Al-pairs for H-ZSM-5 with a Si/Al = 11.5, based on a random statistical distribution of Al atoms (Eq. 3) Lewis type interactions with pyridine were also observed with Co-ZSM-5 (1451 cm^{-1}) and Na-ZSM-5 (1443 cm^{-1}).

temperature cation-exchange to ensure that divalent Co^{2+} accesses all paired sites.[74-75] Similarly, for Co-ZSM-5, only a small fraction of protons (9%) were exchanged at 298 K, while 63% of all available protons were exchanged for Co^{2+} at 353 K, consistent with the expected statistical distribution of paired Al sites (66%, **Table 1**). The drastic change in the fraction of exchanged protons underpins the importance of temperature for metal cation ion-exchange with protonic aluminosilicates; the use of ambient conditions for Co^{2+} ion exchanges significantly underestimates the fraction of paired Al sites.

The approach to equilibrium where all exchangeable protons on paired Al sites was also investigated through successive ion-exchange, where H-ZSM-5 (Si/Al = 11.5) was subjected to successive ion-exchanges with Co at 353 K, ensuring that the fraction of Al pairs was not underestimated by the overall kinetics of ion-exchange. Briefly, H-ZSM-5 was exchanged with a 0.5 M Co solution for 24 hours, dried without a high-temperature calcination, then exposed to a freshly prepared Co solution. No significant trend in the fraction of Al pairs measured via NPA Hofmann elimination was observed with successive Co exchange ($f_{Al,pairs}$ = 63% → 73% → 67%, **Figure 3B**). The consistency with successive ion-exchange is consistent with Gul Hur et al.,[114] where the extent of Co^{2+} exchanged with H-ZSM-5 was unchanged beyond a single ion-exchange. Additionally, the starting cationic form of the zeolite (H-ZSM-5 and NH_4-ZSM-5) led to no significant difference in measured the fraction of protons exchanged by either metal cation (supporting information, sec S7).

3.6. Access to Protons on Co-ZSM-5. Similar to ensuring a more complete extent of ion exchange between metal cations and protons on paired Al sites, it was necessary to determine whether NPA as a probe molecule accessed all residual protons on Co exchanged zeolites. The pores of the MFI framework are more constrained by the presence of metal-cations like Co^{2+} and intraparticle diffusion may impede the access of NPA to residual protonic sites. Even when the zeolite is exposed

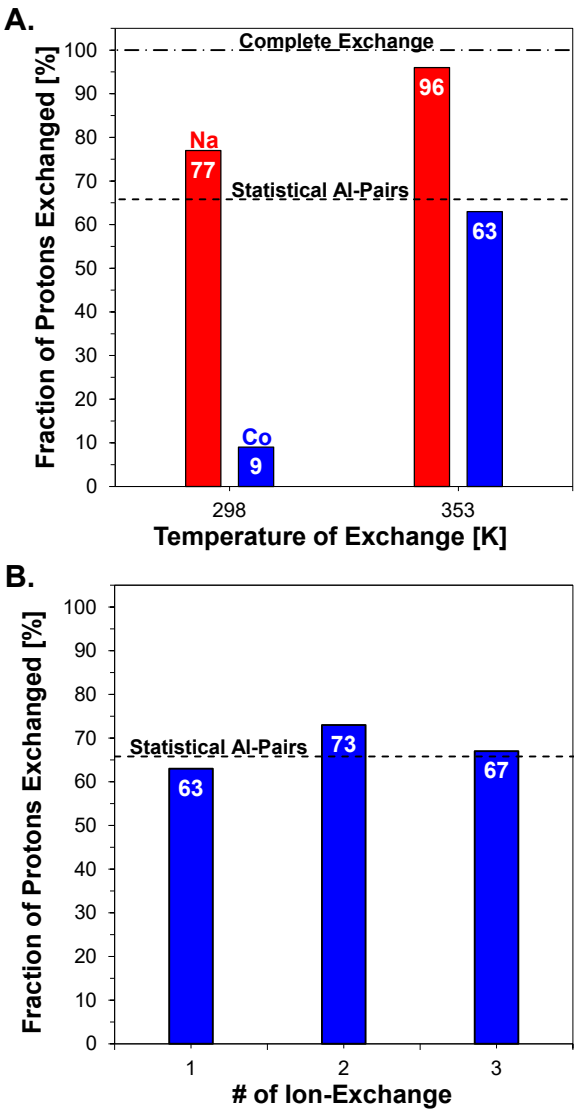

Figure 3. Influence of ion-exchange conditions A. Fraction of protons exchanged with **Na** and **Co** from solution at 298 and 353 K **B.** Fraction of protons exchanged **Co** after multiple ion-exchanges at 353 K; a fresh solution was prepared for each subsequent exchange. Dashed lines indicate complete exchange (**-.-**) for Na-ZSM-5 and the calculated fraction of Al-pairs for H-ZSM-5 with a Si/Al = 11.5 (**---**), based on a random statistical distribution of Al atoms (Eq. 3). Inset numbers indicate the measured fraction of protons exchanged via n-propylamine TPSR. All ion exchanges were performed over a 24-hour period and 0.5 M metal ion concentration.

to a quantity of probe molecule stoichiometrically sufficient to occupy all protonic sites (1 mol RNH_2 per mol H^+), the kinetics of adsorption and/or diffusion into the pore may necessitate a larger molar exposure to ensure complete coverage. Here, we define the extent of exposure as the moles of NPA exposed to the zeolite, normalized by the Al molar content,

$$\text{Extent of Exposure} = \frac{\text{moles of NPA exposed}}{\text{moles of bulk Al in zeolite}} \quad (7)$$

Assuming complete framework incorporation of Al into the zeolite framework, an ideal stoichiometric extent of exposure equal to unity is expected. Indeed, over Co-ZSM-5 with Si/Al = 11.5, 40, and 240, a significantly larger exposure to NPA than the stoichiometric amount was required (**Figure 4**). With increasing exposure to n-propylamine, more protonic sites were probed, resulting in a decreased estimate of the fraction of Al pairs (Eq. 4). Despite the significantly different fraction of paired sites, Al content, and residual density of protonic sites, highly similar trends were observed across the various zeolites. To access all available residual protonic sites in Co exchanged zeolites, approximately an order of magnitude excess in the extent of exposure was required, beyond which no measurable change was observed in the apparent fraction of Al pairs. The required excess is thought to be the result of the intraporous diffusional constraints in the zeolite, and less the presence of Co in the pores; a more than an order of magnitude excess of NPA was similarly required to probe all available protonic sites in H-ZSM-5 (supporting information, **Sec. S6**). Despite the highly favorable adsorption of alkylamines onto the acid sites of H-ZSM-5,[115-116] the overall uptake of alkylamines like pyridine into zeolite cavities has been reported to be diffusion limited.[108, 117] Therefore, to ensure an accurate measurement of the fraction of paired aluminum through alkylamine Hofmann elimination, we employed a two-order-of-magnitude excess extent of exposure (≥ 100 mol NPA per mol Al, **Figure 4**). It is worth noting that the minimum extent of exposure required is likely a function of the zeolite framework and probe molecule identity, and would need to be independently investigated for combinations other than NPA and the MFI framework.

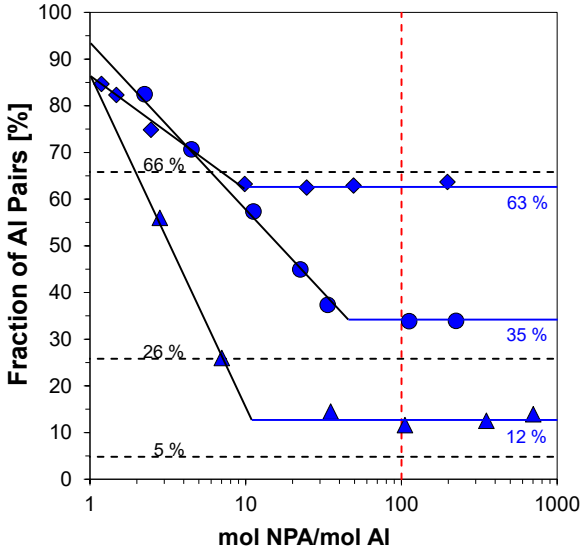

Figure 4. Extent of NPA exposure on Co-ZSM-5. Measured fraction of Al pairs at varying extent of adsorbate exposure (Eq. 7). Red dashed lines show minimum exposure of 100 mol of NPA/mol of Al employed to access all available protonic sites on Co-exchanged ZSM-5, Si/Al = 240 (▲), 40 (●), and 11.5 (♦). Solid lines are to direct the eye.

3.7. Al-pair Site Distribution in MFI. Combining the relevant information discussed in the previous sections, the fraction of Al pairs across a range of Al content (Si/Al = 11.5 – 240) was measured on ZSM-5, with sufficient extent of NPA exposure. Comparing the measured fraction of Al pairs to those predicted based on a random distribution of Al in the framework (Eq. 3), we find excellent quantitative agreement between the two (**Figure 5A**). Despite the wide range of Al content across the various zeolites, within the MFI framework for the commercial samples investigated, incorporation of Al into T-sites appears to follow a random distribution. At most, 63% of the Al incorporated into the MFI

framework appears to be paired (Si/Al). While theoretically an increase in Al content would result in a higher probability of random Al pairing, a limitation is Löwenstein's rule that prevents the existence of Al-O-Al linkages, that can start to form at Si/Al <9.5 for MFI (**Figure 5B**).[16-17, 118] We also observe that MFI samples with less than 1 Al per unit cell, non-trivial fractions of Al pairs will exist (~10%, Si/Al = 140-240), due to framework Al from different unit cells that are close enough to form pairs.[119] Ultimately, the agreement between experimentally measured fraction of paired Al and statistical models helps affirm the utility of n-propylamine as a chemical probe of residual H^+ sites on metal cation-exchanged zeolites.

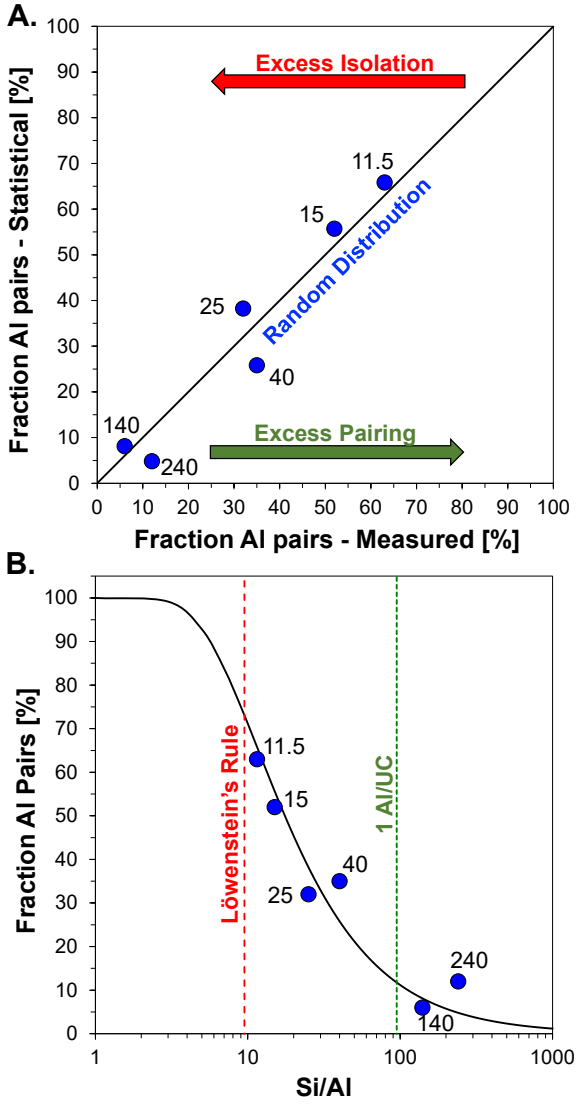

Figure 5. Al-paired site distribution A. Parity plot between randomly distributed (Eq. 3) and measured fraction of Al pairs over a range of Si/Al (11.5-240) in ZSM-5 **B.** Statistical Al-pairs distribution (solid line) with varying Si/Al (1-1000) relative to the measured fraction of Al-pairs (●). The dashed red line indicates the theoretical limit on Al atom framework incorporation as described by Löwenstein's rule. [80, 81] Green dashed line highlights the demarcation where 1 Al/UC exists in the MFI framework [Al/UC = 96/(1+Si/Al)].

4. Conclusion. The effectiveness and extent of metal-cation exchange was quantitatively described through alkylamine Hofmann elimination, which was demonstrated to be a selective probe of protonic sites on the surfaces of distinct forms of ZSM-5. By probing the residual protons of cobalt exchanged ZSM-5 through alkylamine Hofmann elimination, the fraction of Al-pairs was readily determined, regardless of Al content. Accurate quantification of Al pairing was found to be sensitive to both the conditions of ion-exchange and choice of alkylamine probe. Even with elevated metal cation concentrations in exchange solutions (0.5 M) and time allowed for exchange (24 hours), above ambient temperatures were required to achieve complete ion-exchange for both monovalent Na and divalent Co. Commonly employed alkylamines like isopropylamine and tert-butylamine were found to overestimate the density of unexchanged protons on the surface of Na-ZSM-5, attributed to the formation of more-stable carbocations in the course of Hofmann elimination. To probe the extent of ion-exchange more accurately, alkylamines like n-propylamine that undergo Hofmann elimination through a primary carbocation are recommended. Due to significant constraints placed on the diffusion of n-propylamine in the pores of ZSM-5, greater than the stoichiometric exposures of amine were required to completely access all available protons in metal-exchanged zeolites (~100 mol RNH_2 per mol Al). Ultimately, the fraction of Al pairs in the MFI framework was found to follow a random statistical distribution, across a wide

range of Al content (Si/Al 11.5-240). The results presented in this work demonstrate the broad applicability of the reactive probe molecule-based approach to quantify Al-pairs in aluminosilicate zeolites, and for other framework substituted heteroatoms.

Acknowledgements. We acknowledge support from the Center for Plastics Innovation, an Energy Frontier Research Center funded by the U.S. Department of Energy, Office of Science, Office of Basic Energy Sciences under Award number DE-SC0021166. The authors would like to acknowledge Friederike Jentoft for helpful discussions.

Supporting Information. Details of the experimental setup, FT-IR Spectra, and H-ZSM-5 extents of exposure to n-propylamine are available in the supporting information.

Keywords. Hofmann Elimination, Zeolite, Aluminum Pairs, Random Aluminum Distribution, Cobalt Exchange, Alkylamine.

References

1. Chen, H.; Mu, Y.; Shao, Y.; Chansai, S.; Xu, S.; Stere, C. E.; Xiang, H.; Zhang, R.; Jiao, Y.; Hardacre, C.; Fan, X., Coupling non-thermal plasma with Ni catalysts supported on BETA zeolite for catalytic CO2 methanation. *Catalysis Science & Technology* **2019,** 9 (15), 4135-4145.
2. Davis, M. E., Zeolite-based catalysts for chemicals synthesis. *Microporous and Mesoporous Materials* **1998,** 21 (4), 173-182.
3. Metkar, P. S.; Harold, M. P.; Balakotaiah, V., Selective catalytic reduction of NOx on combined Fe- and Cu-zeolite monolithic catalysts: Sequential and dual layer configurations. *Applied Catalysis B: Environmental* **2012,** 111-112, 67-80.
4. Primo, A.; Garcia, H., Zeolites as catalysts in oil refining. *Chemical Society Reviews* **2014,** 43 (22), 7548-7561.
5. Weitkamp, J., Zeolites and catalysis. *Solid State Ionics* **2000,** 131 (1), 175-188.
6. Qiang, Z.; Li, R.; Yang, Z.; Guo, M.; Cheng, F.; Zhang, M., Zeolite X Adsorbent with High Stability Synthesized from Bauxite Tailings for Cyclic Adsorption of CO2. *Energy & Fuels* **2019,** 33 (7), 6641-6649.
7. Velu, S.; Ma, X.; Song, C., Selective Adsorption for Removing Sulfur from Jet Fuel over Zeolite-Based Adsorbents. *Industrial & Engineering Chemistry Research* **2003,** 42 (21), 5293-5304.
8. Wang, Y.; Du, T.; Song, Y.; Che, S.; Fang, X.; Zhou, L., Amine-functionalized mesoporous ZSM-5 zeolite adsorbents for carbon dioxide capture. *Solid State Sciences* **2017,** 73, 27-35.
9. Zanin, E.; Scapinello, J.; de Oliveira, M.; Rambo, C. L.; Franscescon, F.; Freitas, L.; de Mello, J. M. M.; Fiori, M. A.; Oliveira, J. V.; Dal Magro, J., Adsorption of heavy metals from wastewater graphic industry using clinoptilolite zeolite as adsorbent. *Process Safety and Environmental Protection* **2017,** 105, 194-200.
10. Zhan, Y.; Lin, J.; Zhu, Z., Removal of nitrate from aqueous solution using cetylpyridinium bromide (CPB) modified zeolite as adsorbent. *Journal of Hazardous Materials* **2011,** 186 (2), 1972-1978.
11. Yu, L.; Nobandegani, M. S.; Holmgren, A.; Hedlund, J., Highly permeable and selective tubular zeolite CHA membranes. *Journal of Membrane Science* **2019,** 588, 117224.
12. White, J. C.; Dutta, P. K.; Shqau, K.; Verweij, H., Synthesis of Ultrathin Zeolite Y Membranes and their Application for Separation of Carbon Dioxide and Nitrogen Gases. *Langmuir* **2010,** 26 (12), 10287-10293.
13. Ge, Q.; Wang, Z.; Yan, Y., High-Performance Zeolite NaA Membranes on Polymer−Zeolite Composite Hollow Fiber Supports. *Journal of the American Chemical Society* **2009,** 131 (47), 17056-17057.
14. Cui, Y.; Kita, H.; Okamoto, K.-i., Preparation and gas separation performance of zeolite T membrane. *Journal of Materials Chemistry* **2004,** 14 (5), 924-932.
15. Feng, C.; Khulbe, K. C.; Matsuura, T.; Farnood, R.; Ismail, A. F., Recent Progress in Zeolite/Zeotype Membranes. *Journal of Membrane Science and Research* **2015,** 1 (2), 49-72.
16. Larin, A. V., The Loewenstein rule: the increase in electron kinetic energy as the reason for instability of Al–O–Al linkage in aluminosilicate zeolites. *Physics and Chemistry of Minerals* **2013,** 40 (10), 771-780.

17. Loewenstein, W., The distribution of aluminum in the tetrahedra of silicates and aluminates. *American Mineralogist* **1954,** 39 (1-2), 92-96.
18. Rasouli, M.; Yaghobi, N.; Chitsazan, S.; Sayyar, M. H., Effect of nanocrystalline zeolite Na-Y on meta-xylene separation. *Microporous and Mesoporous Materials* **2012,** 152, 141-147.
19. Grande, C. A.; Gascon, J.; Kapteijn, F.; Rodrigues, A. E., Propane/propylene separation with Li-exchanged zeolite 13X. *Chemical Engineering Journal* **2010,** 160 (1), 207-214.
20. Martínez, C.; Corma, A., Inorganic molecular sieves: Preparation, modification and industrial application in catalytic processes. *Coordination Chemistry Reviews* **2011,** 255 (13), 1558-1580.
21. Ma, Z.; Ma, X.; Ni, Y.; Liu, H.; Zhu, W.; Guo, X.; Liu, Z., HZSM-35 zeolite catalyzed aldol condensation reaction to prepare acrylic acid and its ester: Effect of its acidic property. *Chinese Journal of Catalysis* **2018,** 39 (11), 1762-1769.
22. Wang, W.; Jiang, Y.; Hunger, M., Mechanistic investigations of the methanol-to-olefin (MTO) process on acidic zeolite catalysts by in situ solid-state NMR spectroscopy. *Catalysis Today* **2006,** 113 (1), 102-114.
23. Vogt, E. T. C.; Weckhuysen, B. M., Fluid catalytic cracking: recent developments on the grand old lady of zeolite catalysis. *Chemical Society Reviews* **2015,** 44 (20), 7342-7370.
24. Gounder, R.; Iglesia, E., Catalytic Consequences of Spatial Constraints and Acid Site Location for Monomolecular Alkane Activation on Zeolites. *Journal of the American Chemical Society* **2009,** 131 (5), 1958-1971.
25. Sanchez-Castillo, M. A.; Agarwal, N.; Miller, C.; Cortright, R. D.; Madon, R. J.; Dumesic, J. A., Reaction Kinetics Study and Analysis of Reaction Schemes for Isobutane Conversion over USY Zeolite. *Journal of Catalysis* **2002,** 205 (1), 67-85.
26. Herrmann, S.; Iglesia, E., Selective conversion of acetone to isobutene and acetic acid on aluminosilicates: Kinetic coupling between acid-catalyzed and radical-mediated pathways. *Journal of Catalysis* **2018,** 360, 66-80.
27. Huang, X.; Li, H.; Xiao, W.-D.; Chen, D., Insight into the side reactions in methanol-to-olefin process over HZSM-5: A kinetic study. *Chemical Engineering Journal* **2016,** 299, 263-275.
28. Martens, G. G.; Marin, G. B.; Martens, J. A.; Jacobs, P. A.; Baron, G. V., A Fundamental Kinetic Model for Hydrocracking of C8 to C12 Alkanes on Pt/US–Y Zeolites. *Journal of Catalysis* **2000,** 195 (2), 253-267.
29. Kester, P. M.; Crum, J. T.; Li, S.; Schneider, W. F.; Gounder, R., Effects of Brønsted acid site proximity in chabazite zeolites on OH infrared spectra and protolytic propane cracking kinetics. *Journal of Catalysis* **2021,** 395, 210-226.
30. Kamimura, Y.; Iyoki, K.; Elangovan, S. P.; Itabashi, K.; Shimojima, A.; Okubo, T., OSDA-free synthesis of MTW-type zeolite from sodium aluminosilicate gels with zeolite beta seeds. *Microporous and Mesoporous Materials* **2012,** 163, 282-290.
31. Itani, L.; Liu, Y.; Zhang, W.; Bozhilov, K. N.; Delmotte, L.; Valtchev, V., Investigation of the Physicochemical Changes Preceding Zeolite Nucleation in a Sodium-Rich Aluminosilicate Gel. *Journal of the American Chemical Society* **2009,** 131 (29), 10127-10139.
32. Yu, Y.; Xiong, G.; Li, C.; Xiao, F.-S., Characterization of aluminosilicate zeolites by UV Raman spectroscopy. *Microporous and Mesoporous Materials* **2001,** 46 (1), 23-34.
33. Berkson, Z. J.; Hsieh, M.-F.; Smeets, S.; Gajan, D.; Lund, A.; Lesage, A.; Xie, D.; Zones, S. I.; McCusker, L. B.; Baerlocher, C.; Chmelka, B. F., Preferential Siting of Aluminum Heteroatoms in the Zeolite Catalyst Al-SSZ-70. *Angewandte Chemie International Edition* **2019,** 58 (19), 6255-6259.
34. Chizallet, C., Toward the Atomic Scale Simulation of Intricate Acidic Aluminosilicate Catalysts. *ACS Catalysis* **2020,** 10 (10), 5579-5601.
35. García-Pérez, E.; Dubbeldam, D.; Liu, B.; Smit, B.; Calero, S., A Computational Method To Characterize Framework Aluminum in Aluminosilicates. *Angewandte Chemie International Edition* **2007,** 46 (1-2), 276-278.
36. Fang, H.; Kulkarni, A.; Kamakoti, P.; Awati, R.; Ravikovitch, P. I.; Sholl, D. S., Identification of High-CO2-Capacity Cationic Zeolites by Accurate Computational Screening. *Chemistry of Materials* **2016,** 28 (11), 3887-3896.
37. Muraoka, K.; Chaikittisilp, W.; Okubo, T., Energy Analysis of Aluminosilicate Zeolites with Comprehensive Ranges of Framework Topologies, Chemical Compositions, and Aluminum

Distributions. *Journal of the American Chemical Society* **2016,** 138 (19), 6184-6193.
38. Niwa, M.; Suzuki, K.; Katada, N.; Kanougi, T.; Atoguchi, T., Ammonia IRMS-TPD Study on the Distribution of Acid Sites in Mordenite. *The Journal of Physical Chemistry B* **2005,** 109 (40), 18749-18757.
39. Niwa, M.; Katada, N., New Method for the Temperature- Programmed Desorption (TPD) of Ammonia Experiment for Characterization of Zeolite Acidity: A Review. *The Chemical Record* **2013,** 13 (5), 432-455.
40. Selli, E.; Forni, L., Comparison between the surface acidity of solid catalysts determined by TPD and FTIR analysis of pre-adsorbed pyridine. *Microporous and Mesoporous Materials* **1999,** 31 (1), 129-140.
41. Zholobenko, V.; Freitas, C.; Jendrlin, M.; Bazin, P.; Travert, A.; Thibault-Starzyk, F., Probing the acid sites of zeolites with pyridine: Quantitative AGIR measurements of the molar absorption coefficients. *Journal of Catalysis* **2020,** 385, 52-60.
42. Peng, L.; Liu, Y.; Kim, N.; Readman, J. E.; Grey, C. P., Detection of Brønsted acid sites in zeolite HY with high-field 17O-MAS-NMR techniques. *Nature Materials* **2005,** 4 (3), 216-219.
43. Vjunov, A.; Fulton, J. L.; Huthwelker, T.; Pin, S.; Mei, D.; Schenter, G. K.; Govind, N.; Camaioni, D. M.; Hu, J. Z.; Lercher, J. A., Quantitatively Probing the Al Distribution in Zeolites. *Journal of the American Chemical Society* **2014,** 136 (23), 8296-8306.
44. Müller, M.; Harvey, G.; Prins, R., Quantitative multinuclear MAS NMR studies of zeolites. *Microporous and Mesoporous Materials* **2000,** 34 (3), 281-290.
45. Pereira, C.; Gorte, R. J., Method for distinguishing Brønsted-acid sites in mixtures of H-ZSM-5, H-Y and silica-alumina. *Applied Catalysis A: General* **1992,** 90 (2), 145-157.
46. Biaglow, A. I.; Parrillo, D. J.; Kokotailo, G. T.; Gorte, R. J., A Study of Dealuminated Faujasites. *Journal of Catalysis* **1994,** 148 (1), 213-223.
47. Parrillo, D. J.; Adamo, A. T.; Kokotailo, G. T.; Gorte, R. J., Amine adsorption in H-ZSM-5. *Applied Catalysis* **1990,** 67 (1), 107-118.
48. Kresnawahjuesa, O.; Gorte, R. J.; de Oliveira, D.; Lau, L. Y., A Simple, Inexpensive, and Reliable Method for Measuring Brønsted-Acid Site Densities in Solid Acids. *Catalysis Letters* **2002,** 82 (3), 155-160.
49. Feng, R.; Liu, B.; Zhou, P.; Yan, X.; Hu, X.; Zhou, M.; Yan, Z., Influence of framework Al distribution in HZSM-5 channels on catalytic performance in the methanol to propylene reaction. *Applied Catalysis A: General* **2022,** 629, 118422.
50. Li, T.; Chung, S.-H.; Nastase, S.; Galilea, A.; Wang, Y.; Mukhambetov, I.; Zaarour, M.; Navarro de Miguel, J. C.; Cazemier, J.; Dokania, A.; Panarone, L.; Gascon, J.; Cavallo, L.; Ruiz-Martínez, J., Influence of active-site proximity in zeolites on Brønsted acid-catalyzed reactions at the microscopic and mesoscopic levels. *Chem Catalysis* **2023**, 100540.
51. Wang, Y.; Liu, X.; He, X.; Yang, F.; Zhu, X., Tailoring the framework aluminum arrangement in ZSM-5 zeolite to regulate reaction route for alkylation of benzene with methanol. *Microporous and Mesoporous Materials* **2023,** 351, 112491.
52. Wang, Y.; He, X.; Yang, F.; Su, Z.; Zhu, X., Control of Framework Aluminum Distribution in MFI Channels on the Catalytic Performance in Alkylation of Benzene with Methanol. *Industrial & Engineering Chemistry Research* **2020,** 59 (30), 13420-13427.
53. Pham, T. N.; Nguyen, V.; Nguyen-Phu, H.; Wang, B.; Crossley, S., Influence of Brønsted Acid Site Proximity on Alkane Cracking in MFI Zeolites. *ACS Catalysis* **2023,** 13 (2), 1359-1370.
54. Sazama, P.; Dědeček, J.; Gábová, V.; Wichterlová, B.; Spoto, G.; Bordiga, S., Effect of aluminium distribution in the framework of ZSM-5 on hydrocarbon transformation. Cracking of 1-butene. *Journal of Catalysis* **2008,** 254 (2), 180-189.
55. Xing, M.; Chen, Y.; Cao, J.; Han, Y.; Tao, Z.; Wang, F.; Hao, K.; Zhang, L.; Zheng, W.; Xiang, H.; Yang, Y.; Li, Y.; Wen, X., Are olefin aromatization reactions structure sensitive over Al pairs and single Al in H-ZSM-5 Zeolite? *Fuel* **2023,** 333, 126541.
56. Marsden, G.; Kostetskyy, P.; Sekiya, R.-S.; Hoffman, A.; Lee, S.; Gounder, R.; Hibbitts, D.; Broadbelt, L. J., Quantifying Effects of Active Site Proximity on Rates of Methanol Dehydration to Dimethyl Ether over Chabazite Zeolites through Microkinetic Modeling. *ACS Materials Au* **2022,** 2 (2), 163-175.

57. Yuan, Y.; Lobo, R. F.; Xu, B., Ga2O22+ Stabilized by Paired Framework Al Atoms in MFI: A Highly Reactive Site in Nonoxidative Propane Dehydrogenation. *ACS Catalysis* **2022,** 12 (3), 1775-1783.
58. Phadke, N. M.; Van der Mynsbrugge, J.; Mansoor, E.; Getsoian, A. B.; Head-Gordon, M.; Bell, A. T., Characterization of Isolated Ga3+ Cations in Ga/H-MFI Prepared by Vapor-Phase Exchange of H-MFI Zeolite with GaCl3. *ACS Catalysis* **2018,** 8 (7), 6106-6126.
59. Lee, H.; Kim, J.; Song, I.; Jeon, S. W.; Cho, S. J.; Kim, D. H., Controlling the distribution of aluminum in a Cu–zeolite catalyst by seed-assisted synthesis to improve its NH3-SCR activity. *Catalysis Science & Technology* **2022,** 12 (24), 7470-7480.
60. Krishna, S. H.; Goswami, A.; Wang, Y.; Jones, C. B.; Dean, D. P.; Miller, J. T.; Schneider, W. F.; Gounder, R., Influence of framework Al density in chabazite zeolites on copper ion mobility and reactivity during NOx selective catalytic reduction with NH3. *Nature Catalysis* **2023,** 6 (3), 276-285.
61. Chen, L.; Falsig, H.; Janssens, T. V. W.; Jansson, J.; Skoglundh, M.; Grönbeck, H., Effect of Al-distribution on oxygen activation over Cu–CHA. *Catalysis Science & Technology* **2018,** 8 (8), 2131-2136.
62. Dědeček, J.; Čapek, L.; Sazama, P.; Sobalík, Z.; Wichterlová, B., Control of metal ion species in zeolites by distribution of aluminium in the framework: From structural analysis to performance under real conditions of SCR-NOx and NO, N2O decomposition. *Applied Catalysis A: General* **2011,** 391 (1), 244-253.
63. Yang, C.-T.; Janda, A.; Bell, A. T.; Lin, L.-C., Atomistic Investigations of the Effects of Si/Al Ratio and Al Distribution on the Adsorption Selectivity of n-Alkanes in Brønsted-Acid Zeolites. *The Journal of Physical Chemistry C* **2018,** 122 (17), 9397-9410.
64. Moura, P. A. S.; Rodríguez-Aguado, E.; Maia, D. A. S.; Melo, D. C.; Singh, R.; Valencia, S.; Webley, P. A.; Rey, F.; Bastos-Neto, M.; Rodríguez-Castellón, E.; Azevedo, D. C. S., Water adsorption and hydrothermal stability of CHA zeolites with different Si/Al ratios and compensating cations. *Catalysis Today* **2022,** 390-391, 99-108.
65. Findley, J. M.; Ravikovitch, P. I.; Sholl, D. S., The Effect of Aluminum Short-Range Ordering on Carbon Dioxide Adsorption in Zeolites. *The Journal of Physical Chemistry C* **2018,** 122 (23), 12332-12340.
66. Bae, J.; Dusselier, M., Synthesis strategies to control the Al distribution in zeolites: thermodynamic and kinetic aspects. *Chemical Communications* **2023,** 59 (7), 852-867.
67. Wang, S.; He, Y.; Jiao, W.; Wang, J.; Fan, W., Recent experimental and theoretical studies on Al siting/acid site distribution in zeolite framework. *Current Opinion in Chemical Engineering* **2019,** 23, 146-154.
68. Pashkova, V.; Klein, P.; Dedecek, J.; Tokarová, V.; Wichterlová, B., Incorporation of Al at ZSM-5 hydrothermal synthesis. Tuning of Al pairs in the framework. *Microporous and Mesoporous Materials* **2015,** 202, 138-146.
69. Schwalbe-Koda, D.; Kwon, S.; Paris, C.; Bello-Jurado, E.; Jensen, Z.; Olivetti, E.; Willhammar, T.; Corma, A.; Román-Leshkov, Y.; Moliner, M.; Gómez-Bombarelli, R., A priori control of zeolite phase competition and intergrowth with high-throughput simulations. *Science* **2021,** 374 (6565), 308-315.
70. Moliner, M.; Rey, F.; Corma, A., Towards the Rational Design of Efficient Organic Structure-Directing Agents for Zeolite Synthesis. *Angewandte Chemie International Edition* **2013,** 52 (52), 13880-13889.
71. Yokoi, T.; Mochizuki, H.; Namba, S.; Kondo, J. N.; Tatsumi, T., Control of the Al Distribution in the Framework of ZSM-5 Zeolite and Its Evaluation by Solid-State NMR Technique and Catalytic Properties. *The Journal of Physical Chemistry C* **2015,** 119 (27), 15303-15315.
72. Al-Nahari, S.; Dib, E.; Cammarano, C.; Saint-Germes, E.; Massiot, D.; Sarou-Kanian, V.; Alonso, B., Impact of Mineralizing Agents on Aluminum Distribution and Acidity of ZSM-5 Zeolites. *Angewandte Chemie International Edition* **2023,** 62 (7), e202217992.
73. Di Iorio, J. R.; Gounder, R., Controlling the Isolation and Pairing of Aluminum in Chabazite Zeolites Using Mixtures of Organic and Inorganic Structure-Directing Agents. *Chemistry of Materials* **2016,** 28 (7), 2236-2247.
74. Dědeček, J.; Kaucký, D.; Wichterlová, B.; Gonsiorová, O., Co2+ ions as probes of Al distribution in the framework of zeolites. ZSM-5

study. *Physical Chemistry Chemical Physics* **2002,** 4 (21), 5406-5413.
75. Dědeček, J.; Kaucký, D.; Wichterlová, B., Co2+ ion siting in pentasil-containing zeolites, part 3.: Co2+ ion sites and their occupation in ZSM-5: a VIS diffuse reflectance spectroscopy study. *Microporous and Mesoporous Materials* **2000,** 35-36, 483-494.
76. Janda, A.; Bell, A. T., Effects of Si/Al Ratio on the Distribution of Framework Al and on the Rates of Alkane Monomolecular Cracking and Dehydrogenation in H-MFI. *Journal of the American Chemical Society* **2013,** 135 (51), 19193-19207.
77. Bickel, E. E.; Hoffman, A. J.; Lee, S.; Snider, H. E.; Nimlos, C. T.; Zamiechowski, N. K.; Hibbitts, D. D.; Gounder, R., Altering the Arrangement of Framework Al Atoms in MEL Zeolites Using Mixtures of Tetrabutylammonium and Sodium Structure-Directing Agents. *Chemistry of Materials* **2022,** 34 (15), 6835-6852.
78. Nimlos, C. T.; Hoffman, A. J.; Hur, Y. G.; Lee, B. J.; Di Iorio, J. R.; Hibbitts, D. D.; Gounder, R., Experimental and Theoretical Assessments of Aluminum Proximity in MFI Zeolites and Its Alteration by Organic and Inorganic Structure-Directing Agents. *Chemistry of Materials* **2020,** 32 (21), 9277-9298.
79. Chen, K.; Abdolrahmani, M.; Horstmeier, S.; Pham, T. N.; Nguyen, V. T.; Zeets, M.; Wang, B.; Crossley, S.; White, J. L., Brønsted–Brønsted Synergies between Framework and Noncrystalline Protons in Zeolite H-ZSM-5. *ACS Catalysis* **2019,** 9 (7), 6124-6136.
80. Lee, S.; Nimlos, C. T.; Kipp, E. R.; Wang, Y.; Gao, X.; Schneider, W. F.; Lusardi, M.; Vattipalli, V.; Prasad, S.; Moini, A.; Gounder, R., Evolution of Framework Al Arrangements in CHA Zeolites during Crystallization in the Presence of Organic and Inorganic Structure-Directing Agents. *Crystal Growth & Design* **2022,** 22 (10), 6275-6295.
81. Abdelrahman, O. A.; Vinter, K. P.; Ren, L.; Xu, D.; Gorte, R. J.; Tsapatsis, M.; Dauenhauer, P. J., Simple quantification of zeolite acid site density by reactive gas chromatography. *Catalysis Science & Technology* **2017,** 7 (17), 3831-3841.
82. Ho, C. R.; Bettinson, L. A.; Choi, J.; Head-Gordon, M.; Bell, A. T., Zeolite-Catalyzed Isobutene Amination: Mechanism and Kinetics. *ACS Catalysis* **2019,** 9 (8), 7012-7022.
83. Sonnemans, M. H. W.; Den Heijer, C.; Crocker, M., Studies on the acidity of mordenite and ZSM 5. 2. Loss of Broensted acidity by dehydroxylation and dealumination. *The Journal of Physical Chemistry* **1993,** 97 (2), 440-445.
84. Rice, M. J.; Chakraborty, A. K.; Bell, A. T., Al Next Nearest Neighbor, Ring Occupation, and Proximity Statistics in ZSM-5. *Journal of Catalysis* **1999,** 186 (1), 222-227.
85. Liang, T.; Chen, J.; Qin, Z.; Li, J.; Wang, P.; Wang, S.; Wang, G.; Dong, M.; Fan, W.; Wang, J., Conversion of Methanol to Olefins over H-ZSM-5 Zeolite: Reaction Pathway Is Related to the Framework Aluminum Siting. *ACS Catalysis* **2016,** 6 (11), 7311-7325.
86. Song, C.; Chu, Y.; Wang, M.; Shi, H.; Zhao, L.; Guo, X.; Yang, W.; Shen, J.; Xue, N.; Peng, L.; Ding, W., Cooperativity of adjacent Brønsted acid sites in MFI zeolite channel leads to enhanced polarization and cracking of alkanes. *Journal of Catalysis* **2017,** 349, 163-174.
87. Liu, H.; Wang, H.; Xing, A.-H.; Cheng, J.-H., Effect of Al Distribution in MFI Framework Channels on the Catalytic Performance of Ethane and Ethylene Aromatization. *The Journal of Physical Chemistry C* **2019,** 123 (25), 15637-15647.
88. Dědeček, J.; Sobalík, Z.; Wichterlová, B., Siting and Distribution of Framework Aluminium Atoms in Silicon-Rich Zeolites and Impact on Catalysis. *Catalysis Reviews* **2012,** 54 (2), 135-223.
89. Fasano, M.; Bevilacqua, A.; Chiavazzo, E.; Humplik, T.; Asinari, P., Mechanistic correlation between water infiltration and framework hydrophilicity in MFI zeolites. *Scientific Reports* **2019,** 9 (1), 18429.
90. Hendriks, F. C.; Valencia, D.; Bruijnincx, P. C. A.; Weckhuysen, B. M., Zeolite molecular accessibility and host–guest interactions studied by adsorption of organic probes of tunable size. *Physical Chemistry Chemical Physics* **2017,** 19 (3), 1857-1867.
91. Sasca, V.; Avram, L.; Verdes, O.; Popa, A., The n-butyl amine TPD measurement of Brönsted acidity for solid catalysts by simultaneous TG/DTG–DTA. *Applied Surface Science* **2010,** 256 (17), 5533-5538.
92. Biaglow, A. I.; Parrillo, D. J.; Gorte, R. J., Characterization of H,Na-Y Using Amine Desorption. *Journal of Catalysis* **1993,** 144 (1), 193-201.

93. Fletcher Iii, W. P.; Biaglow, A. I., Alkane cracking reactions in zeolites with coadsorbed metal halides. *Catalysis Letters* **1998,** 54 (4), 217-222.
94. Kumar, R.; Cheng, W. C.; Rajagopalan, K.; Peters, A. W.; Basu, P., The Effect of Exchange Cations on Acidity, Activity, and Selectivity of Faujasite Cracking Catalysts. *Journal of Catalysis* **1993,** 143 (2), 594-600.
95. Engelhardt, J.; Hall, W. K., Contribution to the understanding of the reaction chemistry of isobutane and neopentane over acid catalysts, I. *Journal of Catalysis* **1990,** 125 (2), 472-487.
96. Borges, P.; Ramos Pinto, R.; Lemos, M. A. N. D. A.; Lemos, F.; Védrine, J. C.; Derouane, E. G.; Ramôa Ribeiro, F., Activity–acidity relationship for alkane cracking over zeolites: n-hexane cracking over HZSM-5. *Journal of Molecular Catalysis A: Chemical* **2005,** 229 (1), 127-135.
97. Fritz, P. O.; Lunsford, J. H., The effect of sodium poisoning on dealuminated Y-type zeolites. *Journal of Catalysis* **1989,** 118 (1), 85-98.
98. Anderson, B. G.; Schumacher, R. R.; van Duren, R.; Singh, A. P.; van Santen, R. A., An attempt to predict the optimum zeolite-based catalyst for selective cracking of naphtha-range hydrocarbons to light olefins. *Journal of Molecular Catalysis A: Chemical* **2002,** 181 (1), 291-301.
99. Guisnet, M.; Magnoux, P.; Martin, D. In *Studies in Surface Science and Catalysis*, Bartholomew, C. H., Fuentes, G. A., Eds. Elsevier: 1997; Vol. 111, pp 1-19.
100. Trombetta, M.; Armaroli, T.; Gutièrrez Alejandre, A. d.; Ramirez Solis, J.; Busca, G., An FT-IR study of the internal and external surfaces of HZSM5 zeolite. *Applied Catalysis A: General* **2000,** 192 (1), 125-136.
101. Jae, J.; Tompsett, G. A.; Foster, A. J.; Hammond, K. D.; Auerbach, S. M.; Lobo, R. F.; Huber, G. W., Investigation into the shape selectivity of zeolite catalysts for biomass conversion. *Journal of Catalysis* **2011,** 279 (2), 257-268.
102. Cope, A. C.; Trumbull, E. R. In *Organic Reactions*, pp 317-493.
103. Chen, H.; Abdelrahman, O. A., Cooperative Adsorption: Solvating the Hofmann Elimination of Alkylamines. *ACS Catalysis* **2021,** 11 (11), 6416-6430.
104. Qiu, L.; Ying, F. U.; Jinyu, Z.; Nangui, H.; Lijun, L. U.; Xiuzhi, G. A. O.; Mudi, X. I. N.; Yibin, L. U. O.; Yanqiang, S. H. I.; Guangtong, X. U., Investigation on the cation location, structure and performances of rare earth-exchanged Y zeolite. *Journal of Rare Earths* **2017,** 35 (7), 658-666.
105. Gould, N. S.; Xu, B., Effect of liquid water on acid sites of NaY: An in situ liquid phase spectroscopic study. *Journal of Catalysis* **2016,** 342, 193-202.
106. Busca, G., Acidity and basicity of zeolites: A fundamental approach. *Microporous and Mesoporous Materials* **2017,** 254, 3-16.
107. Topaloğlu Yazıcı, D.; Bilgiç, C., Determining the surface acidic properties of solid catalysts by amine titration using Hammett indicators and FTIR-pyridine adsorption methods. *Surface and Interface Analysis* **2010,** 42 (6-7), 959-962.
108. Bludau, H.; Karge, H. G.; Niessen, W., Sorption, sorption kinetics and diffusion of pyridine in zeolites1Dedicated to Professor Lovat V.C. Rees in recognition and appreciation of his lifelong devotion to zeolite science and his outstanding achievements in this field.1. *Microporous and Mesoporous Materials* **1998,** 22 (1), 297-308.
109. Gould, N. S.; Xu, B., Temperature-Programmed Desorption of Pyridine on Zeolites in the Presence of Liquid Solvents. *ACS Catalysis* **2018,** 8 (9), 8699-8708.
110. Buzzoni, R.; Bordiga, S.; Ricchiardi, G.; Lamberti, C.; Zecchina, A.; Bellussi, G., Interaction of Pyridine with Acidic (H-ZSM5, H-β, H-MORD Zeolites) and Superacidic (H-Nafion Membrane) Systems: An IR Investigation. *Langmuir* **1996,** 12 (4), 930-940.
111. Nibou, D.; Mekatel, H.; Amokrane, S.; Barkat, M.; Trari, M., Adsorption of Zn2+ ions onto NaA and NaX zeolites: Kinetic, equilibrium and thermodynamic studies. *Journal of Hazardous Materials* **2010,** 173 (1), 637-646.
112. Inglezakis, V. J.; Loizidou, M. M.; Grigoropoulou, H. P., Ion exchange studies on natural and modified zeolites and the concept of exchange site accessibility. *Journal of Colloid and Interface Science* **2004,** 275 (2), 570-576.
113. Wang, B.; Koike, N.; Iyoki, K.; Chaikittisilp, W.; Wang, Y.; Wakihara, T.; Okubo, T., Insights into the ion-exchange properties of Zn(ii)-incorporated MOR zeolites for the capture of

multivalent cations. *Physical Chemistry Chemical Physics* **2019,** 21 (7), 4015-4021.
114. Hur, Y. G.; Kester, P. M.; Nimlos, C. T.; Cho, Y.; Miller, J. T.; Gounder, R., Influence of Tetrapropylammonium and Ethylenediamine Structure-Directing Agents on the Framework Al Distribution in B–Al–MFI Zeolites. *Industrial & Engineering Chemistry Research* **2019,** 58 (27), 11849-11860.
115. Parrillo, D. J.; Lee, C.; Gorte, R. J., Heats of adsorption for ammonia and pyridine in H-ZSM-5: evidence for identical Brønsted-acid sites. *Applied Catalysis A: General* **1994,** 110 (1), 67-74.
116. Parrillo, D. J.; Gorte, R. J., Characterization of acidity in H-ZSM-5, H-ZSM-12, H-Mordenite, and H-Y using microcalorimetry. *The Journal of Physical Chemistry* **1993,** 97 (34), 8786-8792.
117. Dai, H.; Shen, Y.; Yang, T.; Lee, C.; Fu, D.; Agarwal, A.; Le, T. T.; Tsapatsis, M.; Palmer, J. C.; Weckhuysen, B. M.; Dauenhauer, P. J.; Zou, X.; Rimer, J. D., Finned zeolite catalysts. *Nature Materials* **2020,** 19 (10), 1074-1080.
118. Tang, X.; Liu, Z.; Huang, L.; Chen, W.; Li, C.; Wang, G.; Li, G.; Yi, X.; Zheng, A., Violation or Abidance of Löwenstein's Rule in Zeolites Under Synthesis Conditions? *ACS Catalysis* **2019,** 9 (12), 10618-10625.
119. Knott, B. C.; Nimlos, C. T.; Robichaud, D. J.; Nimlos, M. R.; Kim, S.; Gounder, R., Consideration of the Aluminum Distribution in Zeolites in Theoretical and Experimental Catalysis Research. *ACS Catalysis* **2018,** 8 (2), 770-784.